

On the relationship between Synoptic Wintertime Atmospheric Variability
and path shifts in the Gulf Stream and the Kuroshio Extension

Terrence M. Joyce
Young-Oh Kwon
Lisan Yu

WHOI

2nd Revision 5 Dec. -08
Submitted to J. Climate
Corresponding Author:

Terrence M. Joyce
WHOI, Mail Stop 21
360 Woods Hole Rd.
Woods Hole, MA 02543
tjoyce@whoi.edu

Abstract

Coherent, large scale shifts in the paths of the Gulf Stream (GS) and the Kuroshio Extension (KE) occur on interannual to decadal time scales. Attention has usually been drawn to causes for these shifts in the overlying atmosphere, with some built in delay of up to a few years due to propagation of wind-forced variability within the ocean. Yet these shifts in the latitudes of separated western boundary currents can cause substantial changes in SST, which may influence the synoptic atmospheric variability with little or no time delay. We have chosen to examine various measures of wintertime atmospheric variability in the synoptic band (2:8 days) using a relatively new data set for air-sea exchange (OAFlux) and subsurface temperature indices of Gulf Stream and Kuroshio path that are insulated from direct air-sea exchange and therefore preferable to SST. We find significant changes in the atmospheric variability following changes in the paths of these currents, sometimes in a local fashion such as meridional shifts in measures of local storm tracks, and sometimes non-local, broad regions coincident with and ‘downstream’ of the oceanic forcing. Differences between the N. Pacific (KE) and N. Atlantic (GS) may be in part related to the more zonal orientation of the KE and the stronger SST signals of the GS, but could also be due to differences in mean storm track characteristics over the N. Pacific and N. Atlantic.

1. Introduction

A dynamical relationship must exist that links atmospheric storminess and sea surface fronts like the Gulf Stream (GS) and Kuroshio Extension (KE) since there is geographic relationship in the mean between the pattern of upper tropospheric clouds

and subsurface ocean fronts (Fig. 1). A recent study (Minobe *et al.* 2008) illustrated parts of the link between the mean Gulf Stream position and mean atmospheric structure from the boundary layer up into the upper troposphere. Some studies (e.g. Hoskins and Hodges 2002) of atmospheric variability associated with synoptic signals have concentrated on the variability itself and not with any underlying oceanic feature that might play a role. Others (e.g. Nakamura *et al.* 2004) have also addressed the relationship between the mean oceanic SST and the mean wintertime storm track. That there should be some close relationship between ocean fronts like the GS or KE and mid-latitude winter storm tracks doesn't particularly identify the dynamical cause. Since the system is coupled, there are processes within the atmosphere and the ocean separately which will force an alignment between the two (Hoskins and Valdes 1990, Nakamura *et al.* 2008): storms can produce vorticity fluxes that enhance the mid-latitude zonal jet, which can affect the location of the GS and KE, which can then further influence the development of the storms.

Recently Tanimoto *et al.* (2003) have examined decadal variability in SST and interannual – decadal atmospheric variability for the N. Pacific and Alexander *et al.* (2006) have looked at large scale SST and wintertime storm tracks using both model and reanalysis data. These approaches recognize that interannual - decadal time scale changes in the ocean require one to examine similar time scales for changes in the overlying atmosphere as well. We will follow this line of thinking here, differing in that our focus is interannual - decadal measures of atmospheric *synoptic variability* not variations in seasonal means (e.g., Tanimoto *et al.* 2003, Kelly and Dong 2004). Here we will not

distinguish between storm tracks and baroclinic waveguides (e.g. Wallace, Lim and Blackmon 1988) but will usually refer to them interchangeably as synoptic variability. We will not draw any conclusions about the root cause of the oceanic variability. It is clear that the 22 year record we will be using is insufficient to adequately address the nature of the decadal variability. Rather we will accept the ocean variability as a given and examine whether synoptic atmospheric variability is responding.

We will make use of two rather disparate data sets not used in previous studies of this type. The first of these is a daily, global ocean-atmospheric flux product: OAFlux, (Yu and Weller 2007), which has been augmented (Yu, in preparation) to include surface winds with all variables at sea level (+10m for winds). These products are a combination of observed, satellite-derived fields and ERA-40 and NCEP reanalyses that have been optimally combined using the COARE 3.0 bulk flux algorithm. The OAFlux latent and sensible heat flux estimates are unbiased and the root mean square (rms) difference is less than 8 Wm^{-2} when compared with daily flux time series measurements at 107 locations (Yu *et al.* 2008). The global, ice-free region daily data set that we will use spans roughly a 22 year period from 1983 – 2004, although OAFlux monthly datasets are available online from 1958 to 2006. Because we have daily fields, the data are high passed using a filter similar to that used previously (Alexander *et al.* 2006) to provide variability in a 2-8 day band. We will then examine the rms wintertime variability of different fields from year to year and how they vary in concert with oceanic signals related to but not identical with SST front locations.

The second data set (see also section 3) is the archive of subsurface ocean temperatures which will be used to estimate the spatial mean paths taken by the Gulf Stream (GS) and the Kuroshio Extension (KE) after they have left their respective coastal boundaries. For the Gulf Stream, the archive of subsurface temperature at 200m depth is used. The T(200m) temperature of 15°C has been routinely used to demarcate the north or cold wall of the Gulf Stream for some time (Fuglister 1955) and we have examined smoothed, seasonally resolved locations of this boundary going back to 1955, as discussed in a following section. The leading spatial EOF of this boundary, explaining approximately 50% of the variance, is a north/south shift of the Gulf Stream between 75°W and 55°W, a distance of about 1600 km. A similar procedure with annual resolution was used (Joyce *et al.* 2000) to study the relationship of the Gulf Stream to the NAO and to subtropical mode water. For the Kuroshio Extension between 142°E and 160°E (Qiu *et al.* 2007), an SST-based index was used to examine coupling between the ocean and atmosphere. They resorted to lagged analyses (SST leading) to extract the influence of the ocean on the atmosphere, since the atmosphere will change SST and affect the SST when the ocean is either in phase or slightly following the atmosphere (Frankignoul and Sennéchael 2007). Our Kuroshio Extension index is similar to that derived for the Gulf Stream and is based on the subsurface T(200m) temperature following the seasonally-varying 14°C isotherm, which marks the KE axis (see Kawaii 1972). For both the GS and KE, we will choose the index of wintertime (Jan., Feb., Mar., JFM) position.

2. Mean Atmospheric Fields and Variability Trends

The mean seasonal fields from the basic OAFlux heat flux data have already been discussed by Yu and Weller (2007) elsewhere which also included a discussion of trends and monthly variability. The surface wind products are developed by the Objectively Analyzed air-sea Fluxes (OAFlux) project at WHOI under the auspices of the NASA Ocean Vector Wind Science Team (OVWST) program. The development of global wind analysis is in parallel with the development of ocean evaporation, latent and sensible heat fluxes, and radiative fluxes, and is based on an objective analysis of multiple passive and active microwave sensors (SSM/I, NSCAT, QuikSCAT, AMSR-E) and three atmospheric wind reanalyses. The reanalyzed winds provide directional information for passive microwave wind speed retrievals whenever scatterometer measurements are lacking. Validation of the datasets has been made with 100+ in situ buoy time series measurements. The products include 10-m surface wind (zonal and meridional components and wind speed), wind stress, and wind stress derivative (curl and divergence) fields, and are available on daily basis from mid 1987 to present with two spatial resolutions: 0.25 and 1 degree. To be consistent with the 1-degree analysis of latent and sensible heat fluxes, only the 1-degree resolution winds were used in study.

Here we discuss trends in the band-passed energy, but first show the mean fields for the (relative) vorticity and the divergence, two quantities not previously discussed for this data set. The vorticity (Fig. 2, upper panels) for the N. Atlantic and N. Pacific regions containing the GS and KE shows a mean structure which is rather different for the two regions. In the N. Pacific the strong positive mean vorticity in the atmospheric boundary

layer exists above the subpolar ocean mainly because of decreasing northerly winds (not shown) as one moves eastward into the Aleutian Low. This is not as prominent in the N. Atlantic. In both regions, the speed of the westerlies increases from North to South giving rise to a mid-latitude vorticity maximum which is generally aligned with the axis of the KE and GS. Small scale structures in the mean vorticity and divergence (Fig. 3) near the coasts and near strong SST gradients have been discussed elsewhere by various authors (Chelton *et al.* 2004; Samelson *et al.* 2006; Sampe and Xie 2007; Spall 2007) and are reflected in our results, which also derive from scatterometer wind measurements, although we have used the OAFlux winds at 1X1 degree resolution.

A clear maximum of mean vorticity develops over the GS downstream of Cape Hatteras and the maximum positive vorticity follows the SST front of the GS much closer than for the KE. This positive mean vorticity signature has been ascribed as due to the ocean currents being reflected in the atmosphere boundary layer stress measurements (Chelton *et al.* 2004), and thus in the neutral 10m wind product that we are using. We note that the SST front of the GS is more intense and differs from the broad, diffuse meridional frontal zone of the KE, where the Kuroshio flows eastward from Japan near ca. 35°N and the Oyashio leaves the coast near ca. 40°N. In the N. Atlantic, these two frontal zones are compressed into one, where one passes from subpolar to subtropical waters in a meridional distance of 100km. The GS path also takes an abrupt bend to the north near 50°W as it turns the corner around the Grand Banks. This feature (also clear in Fig. 1) is coincident with atmospheric variables also turning northward, such as latent and sensible heat release (not shown), vorticity and divergence (Fig. 3), as well as their

respective standard deviations in the wintertime synoptic band (lower panels of Fig. 2,3). Thus, wintertime variability in the GS is much less zonal than over the KE in the Pacific. The mean divergence is positive to the north of the KE and GS and negative (convergent) to the south. This is consistent with the mean northerly atmospheric flow across the two currents accelerating over the warm water in the cores of these flows (initially due to boundary layer thickening) and then decelerating on the southerly sides as the atmosphere warms and ‘adjusts’ and the warm ocean SST cores (more prevalent in the GS than the KE) disappear. Regions of large mean sensible heat release to atmosphere correspond well with those regions of convergent motion, as one would expect if the sensible heat release drove upward motion of the air in the atmospheric boundary layer (Lindzen and Nigam 1987). Because this air is moist, due to the co-location of large latent heat release by the ocean, the convergent flow transports water vapor upward and could under the right conditions provide an agent for cloud formation and deeper convection in the atmosphere (Minobe *et al.* 2008). Overall, the synoptic variability of vorticity and divergence exceeds the mean values, unlike the case for latent and sensible heat release, where synoptic variability is roughly 30-50% of the mean wintertime values. For these turbulent heat transport quantities, the variability is clearly strongest where the means are maximum.

One curious finding for the synoptic variability is that there are large trends over the 22 year record (Fig. 4) which are more significant in the N. Pacific than in the N. Atlantic. This is consistent with NWP products and COADS (Chang 2007) and will require that all variables, including the variability measures, need to be de-trended. We

were initially surprised at the strong relationship between the atmospheric variability in the KE and the oceanic KE index (next section) everywhere in the domain until we de-trended the signals. The lower panels of Figs.2 and 3 are not influenced by the existence of the trends in the JFM mean; the trended and detrended versions of the lower panels of Figs.2 and 3 are essentially identical. Clearly the reasons for the trends are of interest but not particularly relevant here. These trends and their spatial characteristics will be discussed in a future study. At this point, we will linearly de-trend all variables to maximize the interannual – decadal signals that are our focus in this study.

3. Gulf Stream and Kuroshio Indices

We have extended the GS path index from earlier work to include seasonally resolved variations. Since the subsurface data for the region are sparse, the data selected (WOD01 updated using GTSPP sources) are centered in the midpoint of each season (eg. JFM for winter) and at each 1X1 degree of latitude/longitude, a time/space ranges of ± 1 year, ± 1 deg. Lat, ± 1 deg. Lon., with a gaussian tapers having an e^2 - folding time scale of $(1 \text{ year})^2$, and spatial scales of $(1 \text{ deg. Lat.})^2$ and $(2 \text{ deg. of Lon.})^2$. Thus the full seasonal signal in the data is substantially smoothed. The gridded temperature data are then used along a path following the mean $T(200\text{m})=15^\circ\text{C}$, or north wall position and 9 points are selected spanning a longitude range from $75:55^\circ\text{W}$. After an EOF analysis, the leading mode is selected, having temperature increasing or decreasing in time at every point along the mean path. This shift of the GS path, is given by the principal component of the leading EOF (Fig. 5), and normalized to have unity

standard deviation. (We have de-trended the temperature data before and EOF analysis and de-trended the leading EOF principal component after EOF analysis with no basic difference in the result). A similar approach but using altimeter data along individual Topex/Poseiden or Jason tracks, detecting the largest gradient of the sea surface anomaly (Kelly and Gille, 1990), was recently employed (Peña-Molino and Joyce 2008) to estimate a spatial mean GS path every month over the satellite period from starting from late 1992. This index, also normalized, agrees well with the longer, but smoother T(200m) estimate. As discussed elsewhere (Frankignoul *et al.* 2001), these two data sources focus on slightly different portions of the GS: one at the north wall, near the maximum SST gradient, the second at the center of the strongest surface flow. However, both give reliable information about the changes in the GS path. It is the longer, subsurface GS path index record which will be used subsequently, selecting out the winter period for a more limited 22 year time window of 1983: 2004 corresponding to the OAFlux product. Satellite altimetric data, though providing better temporal resolution and a more uniform spatial sampling, are presently limited to slightly more than one decade time span, and are too short for the study of decadal variability. In fact, the 22 years for which we have good satellite coverage for the atmospheric variables, is arguably too short as well. However, it is the best we can do today.

A similar, but slightly different approach for deriving an oceanic index was taken for the KE. Here, subsurface temperature, T(200m), was again used spanning a longitude range from 142°E:160°E. The KE index is based on the leading PC of the 14°C isotherm at 200m. The subsurface temperature field was objectively mapped

based on the raw profiles from the World Ocean Database 2005 on seasonal interval and then moving averaged with the 13 months window to mainly retain the annual and longer variability. The data were de-trended prior to the calculation of EOFs. The leading EOF of the 14°C isotherm location at 200m represented uniform north-south shift of the KE and explained about 70% of the total variance. We have also used the vertically-averaged temperature (related to heat content) from the surface to 400m depth and tracked the maximum meridional gradient in this quantity, again using EOF analysis. Both yield similar time series (Fig. 6) and are closer to one another than to a third index, previously published (Qiu *et al.* 2007), which used only SST data within a box extending from Japan all the way to the dateline and covering a latitude range of from 32:38N spanning the KE. As we noted earlier, all three were examined, but the SST index did not produce as robust correlations with the atmospheric data as the other two. In fact, it was for this reason that we sought some other KE index after initially finding relationships between the synoptic variability measures and the KE index were less significant than for the GS. This could possibly be due to the wider span of longitudes defining the SST index in which the KE path may occasionally bifurcate (B. Qiu, personal comm., 2008). Thus, we have selected the $T(200m)=14^{\circ}\text{C}$ one as being both robust and closer to that previously-derived for the GS. The range of path shifts is approximately 100 km, which is a small distance meridionally but coherent over an extensive zonal extent.

4. Relation to Atmospheric Variability

We will present results showing the interannual-decadal relationships between

sea level atmospheric variability and the GS and KE indices separately. By stringing together each of the 22 winters, an interannual time series was constructed containing the standard deviation for each winter of the variability of latent and sensible heat release, meridional winds, vorticity, and divergence, as well as winter estimates of the GS and KE indices. These variability time series were then individually compared and regressed against the ocean-based indices. In effect, we are examining the year-to-year winter atmospheric variability and comparing it to the year-to-year index of wintertime ocean signals that are closely tied to SST gradients. We will show all comparisons for the N. Atlantic and then compare and contrast these results to the N. Pacific.

Gulf Stream

Synoptic variability in the atmosphere can cause widespread outbreaks of cold, dry continental air over the oceans. During these events there are massive heat losses by the ocean into the atmosphere (The CLIMODE Group 2008). Since these turbulent exchanges produce large latent and sensible fluxes across the air-sea interface, they provide energy to cool the oceanic waters which move northward from the subtropics and after heat release, warm the overlying atmosphere. These processes, which are sensitive to temperature differences between the air and water, are expected to play a role in the air-sea coupling, thus linking atmospheric variability and GS (and KE) path location. There could be other oceanic signals (frontal strength, surface transport) that are important, but here we choose only to examine the path changes, for which a meridional shift would create a large perturbation in the SST field seen by the

atmosphere. For latent heat flux variability (Fig. 7), the interannual change in the variability index is roughly 10-20% of the mean (compare upper and lower left panels of Fig. 7). The correlation pattern between the variability and GS index indicates a dipole structure on either side of the mean GS, consistent with the atmospheric boundary layer signal shifting northward (or southward) in phase with the GS. We show only correlations that are significant at the 90% significance level and also show the regression of the atmospheric signal onto the ocean index. Because the latter has a rms value of 1, the regression shows the amplitude of the atmospheric boundary layer signal that is explained by one standard deviation of the index path shifts. Since the independent variable in our regression is a measure of atmospheric variability, and this is uncorrelated with the value in the previous or following winter, we have estimated significance based on the 22 independent winter records in the time series (20 degrees of freedom after mean and trend removal). The amplitude of the local latent heat flux regression is $\sim 5 \text{ Wm}^{-2}$, which broadens the latent heat loss when the GS is north, and intensifies the local maximum south of the GS when the GS is south. The dipole signal cancels out in a spatial mean to first order and merely represents a change in the location of the latent heat loss depending on the location of the GS. There is also a curious correlation signal outside of the ‘storm track’ in the subtropics at around 30°N . This is not a ‘local’ response to path shifts. We have also carried out composite analyses in this and other comparisons (not shown) and arrived at similar conclusions. Other atmospheric signals (below) will have a similar ‘non local’ signal in this location.

Similar patterns for the sensible heat exchange (Fig. 8) are also found. However

the mean (not shown) and mean rms (upper left panel) show large values immediately next to the shoreline, and there is not a clear maximum over the GS as for latent heat. This reflects the fact that the evaporation over the colder, nearshore waters is suppressed compared to farther offshore where both the atmospheric boundary layer and the ocean are warmer and the air can hold more water vapor. Because of this difference between the sensible and latent heat patterns, the correlation pattern of the interannual variability does not suggest a simple dipole, but rather an extension of the high sensible heat loss variability to the south when the GS path is in a southerly location. Again we see a non-local response in the atmosphere around 30°N.

Meridional wind variability, often examined in storm track analyses, has a broad variability maximum located to the south of the mean GS path (Fig. 9). As the GS shifts northward, a shift of this mean pattern to the north would clearly bring stronger variability of meridional winds to this region, while a southward shift of the variability maximum following the GS would not necessarily bring stronger variability to the region immediately south of the mean GS path, because of the broad meridional maximum in this variability measure. We believe this explains the local correlation patterns in Fig. 9. A non-local response in the eastern part of the domain is not clearly related to shifts in a variability pattern, but rather to the diversion of more atmospheric variability towards the Azores (38°N, 28°W), just off our map to the east, when the GS is in a southerly location. It is also seen in the zonal wind variability (not shown). This non-local wind response is not co-located with those for the turbulent heat fluxes.

Both vorticity (Fig. 10) and divergence (Fig. 11) are ‘noisier’ than other variables presented thus far , since smaller scale atmospheric variability is enhanced when derivatives are taken of the synoptic scale flow. The mean divergence variability maximum is somewhat more meridionally constrained than for vorticity, but both closely follow the mean GS path. And it is apparent that they track northward and southward with path changes, based on the spatial pattern of the correlations in the vicinity of the GS. There is also a hint that in the SE part of the domain, there is an increase of both of these variability measures as the GS path is southerly. There is also a similarity to the non-local response of the turbulent fluxes near 30°N, 60°W.

Because the region to the north of the GS path is relatively narrow, any given synoptic system in the atmosphere that passes over this region will be at least partly over land. Thus, the atmospheric region to the north of the mean GS is substantially different than for the KE in the N. Pacific, where the entire region is maritime. And there is no Atlantic counterpart to the Sea of Japan/East Sea in the ‘upstream’ region of the Atlantic storm tracks. We believe these geographic differences are important for the difference in response in the atmospheric variability for the two regions.

Kuroshio Extension

Unlike the GS region, the relationship of the latent heat variability (Fig. 12) with the KE index is quite different: downstream of the region which defines our KE index, the variability is significantly higher (lower) when the KE is in a northerly (southerly) position.

We define our KE index in the region between 142°E and 160°E . There is no suggestion of a local response that follows the current (dipole) as the KE shifts in time. This is also true for the sensible heat variability (Fig. 13), although not as widespread. So unlike the GS, the spatial mean signal in the KE is one of more turbulent heat loss when the KE is in a northerly position and visa versa for a southerly position. And there seems to be an upstream influence of the KE in the waters surrounding the Korean peninsula and substantial variability throughout the East Sea/Sea of Japan. As for the GS, however, the meridional maximum in sensible heat variability is shifted northward compared to that for latent heat and the maximum region for variability in meridional winds (Fig. 14) is centered over but south of the mean KE axis. Thus northward shifts of the winds in concert with the KE will produce a local signal to the north of the KE, but not to the south, since southward shifts of the wind maximum following the KE can produce both signs of correlations depending location. Also, as for the GS, there is an increase of meridional wind variability with southward shifts of the KE in the SE part of the domain, suggesting remote shifts of storm tracks with little or no affects on the thermodynamics of the air-sea exchange. The vorticity map (Fig. 15) is quite interesting and shows the importance of the dual frontal zone east of Japan. The mean variability is broad and generally shows a high slanting ENE from the point where the KE is closest to Japan. Yet the part of the signal that varies from year to year (lower left panel of Fig. 15) indicates that this tracks over the subarctic front or eastward extension from Japan of the Oyashio. It is possible that this oceanic front may move independently from the KE. We have not examined this here. It is quite apparent that despite the patchiness of the significant correlations between vorticity variability and the KE path, there is a clear sign

change in their correlation across the mean KE path. Clearly, the atmospheric boundary layer vorticity variability changes in concert with the KE location, independent of any pre-existing alignment between the KE and ‘mean rms vorticity’ signal. Again, we stress that an SST or subsurface temperature index for the subarctic front might show statistical relationships with the atmospheric vorticity variability that are different than for the KE. This is something for future study.

5. Discussion

The relationship between the observed vorticity and divergence can be illuminated by the use of a simple model of the Marine Atmospheric Boundary Layer (MABL) where we consider layer velocities (u, v) that obey a balance of

$$\begin{aligned} fu &= -\rho^{-1} p_y - rv, \\ -fv &= -\rho^{-1} p_x - ru, \\ \text{where } r &= C_d |(u_l, v_l)| / H, \end{aligned}$$

where f is the (constant) Coriolis parameter and r is a (constant) ‘Rayleigh’ friction, representing the ocean/atmosphere stress acting over the layer of depth H with velocity (u, v) . Here we have used a linearized form of the quadratic bottom stress based around a velocity (as yet unspecified) of (u_l, v_l) . The two equations above can be differentiated to obtain two related equations:

$$\begin{aligned} f(v_x - u_y) &= \rho^{-1}(p_{xx} + p_{yy}) + r(u_x + v_y), \\ f(u_x + v_y) &= -r(v_x - u_y). \end{aligned}$$

The second illustrates the relationship between the vertical component of vorticity and the horizontal divergence of the boundary layer velocity: namely that they are linearly related with divergence scaled by a factor of $(-r/f)$ times the vorticity. The first and second can be used to relate the horizontal laplacian of pressure to the vorticity. In the above, we have assumed that the pressure will not be affected by boundary layer processes as might be expected from heating or cooling (e.g. Lindzen & Nigam 1987). But the above simple relationship between vorticity and divergence can be used to explain the main features in the observations of the previously presented mean quantities (Figs. 2, 3) as well as for the band-passed data. If the mean vorticity and divergence are taken from a selected area over the Gulf Stream (Figs. 2 & 3, boxed region) characterized by its location within the rms vorticity and divergence maximum for the 2-8 day band, we estimate that the ratio of the mean divergence and vorticity is $\sim - .48$. Thus, friction is an $o(1)$ quantity in the MABL. For the variability in the 22 winter records, we have constructed a joint probability distribution function (*pdf*) from the scatter plot of the band-passed vorticity and divergence in the storm track maximum region of the Gulf Stream (Fig. 16). We find for this region that the appropriate non-dimensional factor relating divergence and vorticity is $\sim -.78 \pm .06$ for the band-passed data (95% confidence interval following Garrett and Petrie (1981), using our estimated degrees of freedom). One might expect this ratio to be the same for mean flow and variability if it truly represents the simple MABL model above. But because the underlying physics of the drag law upon which the frictional parameterization is based is quadratic, the ratio might vary between the mean and synoptic states. We believe, however, that there is a simpler explanation for the difference in the two ratios: neglect of

the imprint of the mean flow of the Gulf Stream on the overlying mean atmosphere (Cornillon and Park 2001). With a mean NW'ly air flow giving a downstream flow of wind over water, the GS will produce a negative imprint of its vorticity on the MABL vorticity. Since the mean MABL vorticity is small compared to the fluctuations and comparable to the ocean-induced signal, one sees an increase in the magnitude of the positive mean vorticity south of the GS and over the region where we have examined this ratio for the mean state and for the fluctuations.

Beyond these issues, note that the scatter of the synoptic vorticity and divergence data is quite skewed, with an enhanced tail associated with *positive* vorticities and *convergent flows*: clearly what one would expect from intense, cyclones with convergent Ekman layers that aid in their development. For variability in this quadrant (SE of the scatter plot in Fig. 16) of the bivariate distribution, the percent of the total variance explained would be 25% for a symmetric *pdf* with 2 independent variables. However, we find 51% (55%) of the total variance of vorticity (divergence) is contained in this quadrant due to a higher probability of extreme events. The NE and SW quadrants together explain only about 20% of the variance. To this extent, therefore, our statistical relationships deriving from the covariability between storm signals and GS/KE paths tend to be dominated by convergent wintertime cyclones with weaker, divergent anticyclones, at least over the region where the mean variability signals are largest.

Our analysis of atmospheric variability has been limited by our data to the sea surface, within the MABL. It remains a question how connected the MABL variability is

with the rest of the troposphere. That there is an active connection based on the mean fields seems to be established, at least for the GS region (Minobe *et al.* 2008). Oceanic heating of the MABL in synoptic storms is a vigorous signal and makes up a significant portion of the mean wintertime signal. Our results indicate that rms, storm-related sensible and latent fluxes of 60 and 90 Wm⁻², respectively, are found over the GS (Figs. 8, 7) and that these are appreciable in terms of mean values, approaching 30-50% of the mean turbulent fluxes. Similar results apply to the KE region. Thus, winter storms must contribute significantly to the mean signal of diabatic heating throughout the troposphere over the GS & KE and to the energetics which creates the storm tracks in the first place (Hoskins and Valdes 1990). But the vorticity dynamics of the variability also leads to a reinforcement of the westerly wind jet which, at sea level, can influence the mean latitudes of the oceanic western boundary currents once they leave the coasts. This conundrum of what causes what is partially removed by looking at the *variability* of the ocean fronts. Because they exhibit path changes on interannual to decadal time scales, observing the co-variability of the MABL variability and the GS and KE path locations at zero seasonal lag should enhance the oceanic signals which force the atmosphere. At time lags of one to several years, the oceanic variability caused by the atmosphere will dominate, as has already been established for the KE and GS. That there is a significant change in atmospheric variability in concert with the changes in the GS and KE paths with no appreciable seasonal lag suggests that the ocean is forcing the atmospheric storm track and that there might be skill in predicting future changes of atmospheric storm tracks based on oceanic conditions looking ahead several months to a year. By itself, the rms variability of the atmospheric variables has no persistence from one

season to the next.

The effect of the changing GS and KE path on the overlying atmospheric variability is not the same for both regions, perhaps because of differences in the mean storm tracks, rather than the mean ocean. However, the magnitude of the mean SST gradient in the KE and GS is different (Figs. 2, 3) as is the response of the SST to changes in the GS and KE paths (Fig. 17). The spatial structure of the SST signal associated with changes in these indices is different for the two regions. For the GS, the associated SST signal looks like more north/south shifts of the GS itself, but with a larger amplitude to the north of the GS than to the south, due to the fact that the SST gradient is larger on the northern flank of the warm core than to the south. For the KE, the SST signal is broad, downstream, and reflects a warmer KE region when the KE itself is north and colder when south. These dominant SST signals for the GS and KE are damped by the atmospheric response rather than generated by changes in the storm track: they are of the same sign as changes in storm-related latent and sensible heat flux: increased (decreased) heat loss over warmer (colder) waters.

For both regions defining the northern hemisphere storm tracks, the local, frontal signatures of oceanic forcing of synoptic atmospheric variability are limited to within a few degrees of latitude on both sides of the mean SST fronts. However, we have also found non-local signals in the atmosphere which suggest that changes in GS and KE path location can influence broad regions of the atmospheric storm climate ‘downstream’ of the regions of coherent path changes in these currents. The atmospheric boundary layer signals are not always consistent among the variables measured in relation to the

oceanic forcing. For example, latent heat release behaves differently in the far field than meridional wind or vorticity variability. The reasons for this as well as the non-local nature of the response are not entirely clear to us at this time. They may in part be due to SST-related forcing by shifts of the ocean fronts, but also due to seasonal-decadal changes in the low frequency atmospheric circulation arising from its response to oceanic forcing and not a direct link between path changes and large-scale, non-local synoptic variability. Some of these issues can be examined using existing data sets, but one would hope that further dynamical connections can be made using models that both resolve the strong SST gradients of these oceanic flows and allow them to shift in a coherent fashion over substantial zonal distances.

6. Acknowledgements

Two of us (T J, Y-O K) became interested in this topic as a result of our participation in a US CLIVAR working group on the role of separated western boundary currents on air-sea exchange and climate variability (<http://www.usclivar.org/wbc.php>) and because of the maturing of two ongoing CLIVAR process studies on the Kuroshio Extension (KESS: <http://uskess.org/>) and Gulf Stream (CLIMODE: www.climode.org). Support for this work from various grants [T.Joyce.: NSF OCE-0424865, Y.-O. Kwon.: The Grayce B. Kerr Fund and The Jessie B. Cox Endowed Fund, L.Yu.: NOAA NA17RJ1223 and NASA Vector Wind Science Team through JPL subcontract 1283726] is gratefully acknowledged.

References

- Alexander, M. and Coauthors, , 2006: Extratropical Atmosphere–Ocean variability in CCSM3. *Journal of Climate*, **19**, 2496-2525.
- Chang, E. K. M., 2007: Assessing the increasing trend in Northern Hemisphere winter storm track activity using surface ship observations and a statistical storm track model. *Journal of Climate*, **20**, 5607-5628.
- Chelton, D. B., M. G. Schlax, M. H. Freilich, and R. F. Milliff, 2004: Satellite measurements reveal persistent small-scale features in Ocean winds. *Science*, **303**, 978-983.
- Cornillon, P., and K.-A. Park (2001), Warm Core Ring velocities inferred from NSCAT, *Geophys. Res. Lett.*, **28**(4), 575-578.
- Frankignoul, C., G. de Coëtlogon, T. M. Joyce, and S. Dong, 2001: Gulf Stream variability and Ocean–Atmosphere interactions*. *Journal of Physical Oceanography*, **31**, 3516-3529.
- Frankignoul, C., and N. Sennéchael, 2007: Observed influence of North Pacific SST anomalies on the Atmospheric Circulation. *Journal of Climate*, **20**, 592-606.
- Fuglister, F.C., 1955. Alternate analyses of current surveys. *Deep-Sea Res.*, **2**, 213-229.
- Garrett, C., and B. Petrie, 1981: Dynamical aspects of the flow through the Strait of Belle Isle. *J. Phys. Oceanogr.*, **11**, 376–393.
- Hoskins, B.J., and P.J. Valdes, 1990: On the existence of storm-tracks. *J. Atmos. Sci.*,

47, 1854–1864.

Hoskins, B. J., and K. I. Hodges, 2002: New perspectives on the Northern Hemisphere winter storm tracks. *Journal of the Atmos. Sci.*, **59**, 1041-1061.

Joyce, T. M., C. Deser, and M. A. Spall, 2000: The relation between decadal variability of Subtropical Mode Water and the North Atlantic Oscillation*. *Journal of Climate*, **13**, 2550-2569.

Kelly, K. A., and S. T. Gille (1990), Gulf Stream surface transport and statistics at 69°W from the Geosat Altimeter, *J. Geophys. Res.*, 95(C3), 3149–3161.

Kelly, K.A. and S. Dong, 2004: The relationship of western boundary current heat transport and storage to mid-latitude ocean-atmosphere interaction, in *Earth's Climate: The Ocean-Atmosphere Interaction*, edited by C. Wang, S.-P. Xie, and J. A. Carton, pp. 347-363, American Geophysical Union Geophysical Monograph 147.

Lindzen, R. S., and S. Nigam, 1987: On the role of Sea Surface Temperature gradients in forcing low-level winds and convergence in the Tropics. *J. Atmos. Sci.*, **44**, 2418-2436.

Minobe, S., A. Kuwano-Yoshida, N. Komori, S. Xie, and R. J. Small, 2008: Influence of the Gulf Stream on the troposphere. *Nature*, **452**, 206-209.

Nakamura, H., T. Sampe, Y. Tanimoto, A. Shimpo, and AGU, 2004: *Observed associations among storm tracks, jet streams, and midlatitude oceanic fronts*.

Earth's Climate: The Ocean-Atmosphere Interaction. Geophysical Monograph,
Amer. Geophys. Union, 329 pp.

Nakamura, H., T. Sampe, A. Goto, W. Ohfuchi, and S.-P. Xie (2008), On the importance
of midlatitude oceanic frontal zones for the mean state and dominant variability in
the tropospheric circulation, *Geophys. Res. Lett.*, 35, L15709,
doi:10.1029/2008GL034010.

Peña-Molino, B., and T. M. Joyce (2008), Variability in the Slope Water and its relation to
the Gulf Stream path, *Geophys. Res. Lett.*, 35, L03606,
doi:10.1029/2007GL032183.

Qiu, B., N. Schneider, and S. Chen, 2007: Coupled decadal variability in the North
Pacific: An observationally constrained idealized model*. *Journal of Climate*, **20**,
3602-3620.

Samelson, R. M., E. D. Skillingstad, D. B. Chelton, S. K. Esbensen, L. W. O'Neill, and
N. Thum, 2006: On the Coupling of wind stress and Sea Surface Temperature.
Journal of Climate, **19**, 1557-1566.

Sampe, T., and S. Xie, 2007: Mapping high sea winds from space. *Bull. Amer. Meteor. Soc.*, **88**, 1965-1978.

Schiffer, R.A., and W.B. Rossow, 1983: The International Satellite Cloud Climatology
Project (ISCCP), the first project of the World Climate Research Program. *Bull.*

- Amer. Meteor. Soc.*, 64, 779-784.
- Song, Q., P. Cornillon, and T. Hara, 2006, Surface wind response to oceanic fronts, *J. Geophys. Res.*, 111, C12006, doi:10.1029/2006JC003680.
- Spall, M. A., 2007. Midlatitude wind stress–Sea Surface Temperature coupling in the vicinity of oceanic fronts. *Journal of Climate*, **20**, 3785-3801.
- Tanimoto, Y., H. Nakamura, T. Kagimoto, and S. Yamane, 2003. An active role of extratropical sea surface temperature anomalies in determining anomalous turbulent heat flux, *J. Geophys. Res.*, 108(C10), 3304, doi:10.1029/2002JC001750.
- The Climode Group, 2008. Observing the cycle of convection and restratification over the Gulf Stream system and the subtropical gyre of the North Atlantic ocean: preliminary results from the CLIMODE field campaign. *Bull. Amer. Meteor. Soc.*, accepted.
- Wallace, J. M., G. Lim, and M. L. Blackmon, 1988: Relationship between cyclone tracks, anticyclone tracks and baroclinic waveguides. *J. Atmos. Sci.*, **45**, 439-462.
- Yu, L., and R. A. Weller, 2007: Objectively analyzed air–sea heat fluxes for the global ice-free oceans (1981–2005). *Bull. Amer. Meteor. Soc.*, **88**, 527-539.
- Yu, L., X. Jin, and R. A. Weller, 2008: Multidecadal global flux datasets from the

Objectively Analyzed Air-sea Fluxes (OAFlux) Project: latent and sensible heat fluxes, ocean evaporation, and related surface meteorological variables.
Woods Hole Oceanographic Institution, OAFlux Project Technical Report.
OA-2008-01, 64pp. Woods Hole. Massachusetts. Available online at
<http://oaflux.whoi.edu/>

Figure Captions

Figure 1. Climatological (or time mean) distribution of per cent cloudiness (colors) in high (IR) clouds from ISCCP cloud climatology (Schiffer and Rossow, 1983) from 1983-2006. Subsurface 200m temperature is contoured every 5°C from 0 to 20. Where the 5 to 15°C isotherms are tightly grouped demarks the pathways of the Gulf Stream and the Kuroshio Extension, which underlie the high cloud maxima.

Figure 2. Time-mean (relative) vorticity from the OAFlux surface wind climatology for JFM for regions of the KE (upper left) and GS (upper right), with the rms synoptic, band-passed variability for JFM for each region in the respective lower panels. The black contours are the climatological JFM mean SST with 2°C interval. Vorticity units (colors) are in 10^{-6} s^{-1} . A box selected for later analysis of variability (Fig. 16) over the storm track maximum is indicated in the lower right panel.

Figure 3. As for Fig. 2 but for horizontal divergence. Note how the mean fields mirror the vorticity pattern with approximately the same magnitude.

Figure 4. For the spatial regions shown in Figs. 2 and 3 ($24.5:50.5\text{N}$, $-85.5:-34.5$, or $124.5:175.5\text{E}$), the winter root mean square (rms) synoptic variability in surface wind speed is plotted for the 22 year OAFlux record period. The solid lines are for the KE, the dashed for the GS. Smoothed interannual variability (with a symmetric, low-passed butterworth filter) is plotted with thicker lines to reduce interannual variability and better show the trends in the N. Pacific data. Linear trends using the unfiltered data are also

shown.

Figure 5. Normalized time series of the principal component of the GS latitude shift based upon subsurface temperature T(200m) (dashed line), and satellite altimeter (solid line). Each of these PCs represent the leading EOF mode of seasonal (T200m) or monthly (altimeter) variability for the GS path. Only the JFM record for T(200m) PC was used in our analysis.

Figure 6. Normalized time series of KE path changes based upon SST (solid line), T(200m) (dashed line), and T(0:400m) (dotted line) subsurface temperatures as discussed in text.

Figure 7. Latent heat flux for the GS region: mean rms 2:8 day band for JFM (upper left), interannual JFM std of rms 2:8 day band (lower left), correlation coefficient of interannual JFM rms variability with GS index (upper right) with only significant (>90%) values plotted, and regression against GS index (lower right). Darker shades of gray denote regions of positive correlation/regression here and elsewhere, while lighter shades of gray are negative. For all but the correlation coefficient, the units are in Wm^{-2} . The mean GS path is plotted as the solid line in all panels. The contour interval for the correlation coefficient (upper right) is 0.1 and for the regression is 0.1 times the gray scale maximum on the plot (lower right).

Figure 8. As in Fig. 7 but for sensible heat flux.

Figure 9. As in Fig. 7 but for meridional wind. In this case the units are in ms^{-1} .

Figure 10. As in Fig. 7 but for vorticity. For upper left panel, the scale is in 10^{-5} s^{-1} , while the scales for the lower left and lower right are in 10^{-6} s^{-1} .

Figure 11. As for Fig. 10 but for divergence.

Figure 12. Latent heat flux for the KE region: mean rms 2:8 day band for JFM (upper left), interannual JFM std of rms 2:8 day band (lower left), correlation coefficient of interannual JFM rms variability with KE index (upper right) with only significant (>90%) values plotted, and regression against KE index (lower right). For all but the correlation coefficient, the units are in Wm^{-2} . The mean KE path is plotted as the solid line in all panels.

Figure 13. As in Fig. 12 but for sensible heat flux.

Figure 14. As in Fig. 12 but for meridional winds. In this case the units are in m s^{-1} .

Figure 15. As in Fig. 10 but for vorticity in the KE region.

Figure 16. For the storm track maximum box over the GS (see Figs. 2, 3), we show a

scatter plot of 2-8 day band-passed divergence and vorticity, with regression lines and % of variance explained by observations in each of the 4 quadrants of the plot (upper panel).

The solid lines in the upper panel are regressions for one variable against the other.

Along the neutral regression line (dashed in upper panel), we show the histogram of vorticity (lower panel) indicating a skewed distribution. Here we have filtered the data and removed the means, so the mean vorticity and divergence is zero. The means of these quantities are displayed in Figs. 2, 3, respectively.

Figure 17. Wintertime SST signals are correlated with the KE and GS indices to show the effect of these frontal shifts on SST. The correlation coefficient (upper panels) is plotted for significant (>90% confidence) correlations and the regression ($^{\circ}\text{C}$, lower panels) is shown for the KE region (left panels) and GS (right panels). The contour interval for all panels is 0.1 in the respective units.

Figure 1. Climatological (or time mean) distribution of per cent cloudiness (colors) in high (IR) clouds from ISCCP cloud climatology (Schiffer and Rossow, 1983) from 1983-2006. Subsurface 200m temperature is contoured every 5°C from 0 to 20. Where the 5 to 15°C isotherms are tightly grouped demarks the pathways of the Gulf Stream and the Kuroshio Extension, which underlie the high cloud maxima.

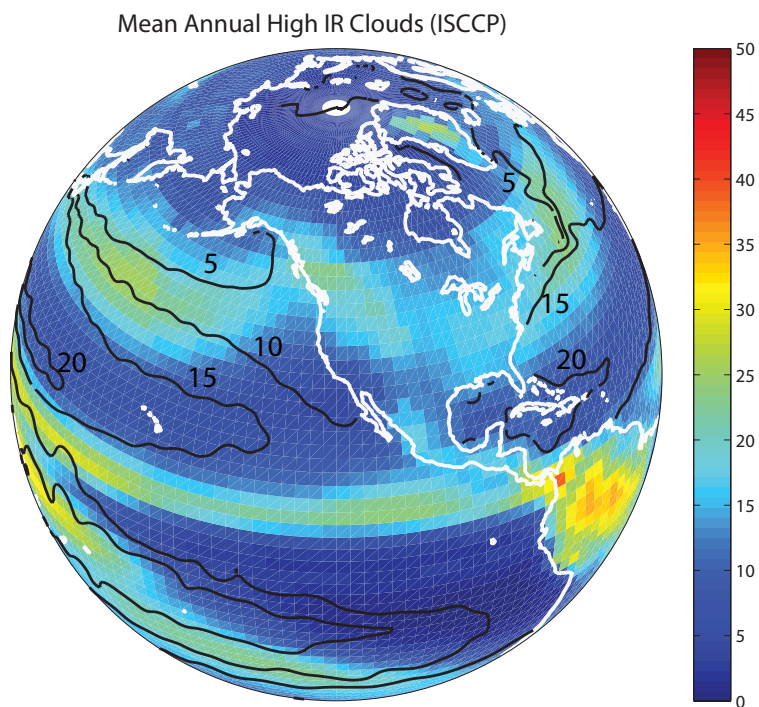


Figure 2. Time-mean (relative) vorticity from the OAFlux surface wind climatology for JFM for regions of the KE (upper left) and GS (upper right), with the rms synoptic, band-passed variability for JFM for each region in the respective lower panels. The black contours are the climatological JFM mean SST with 2°C interval. Vorticity units (colors) are in 10^{-6} s^{-1} . A box selected for later analysis of variability (Fig. 16) over the storm track maximum is indicated in the lower right panel.

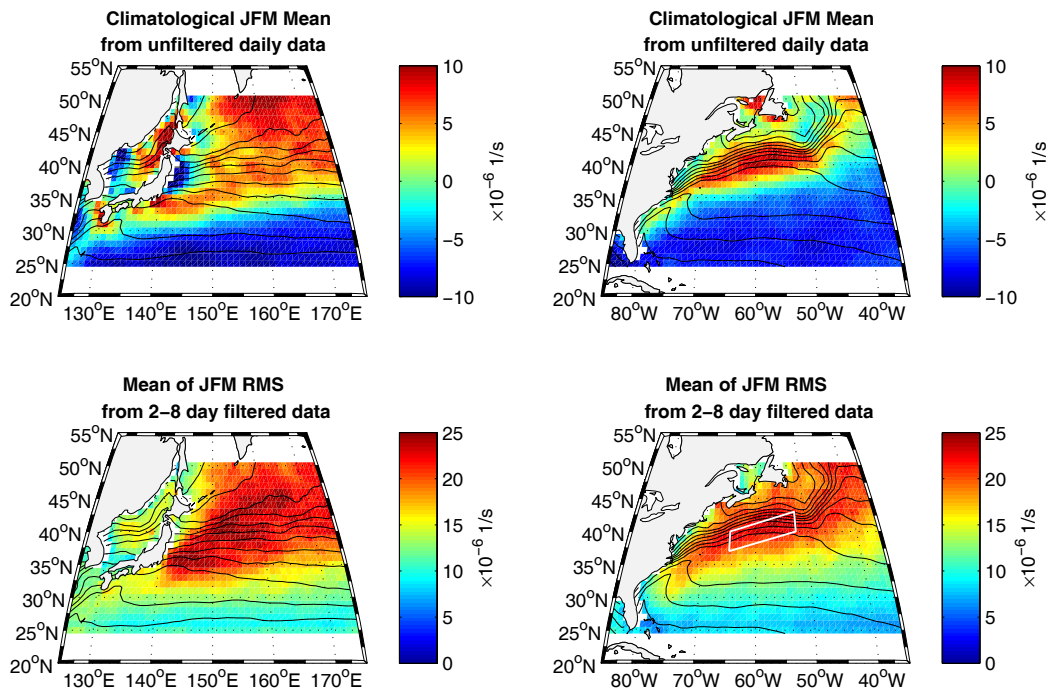


Figure 3. As for Fig. 2 but for horizontal divergence. Note how the mean fields mirror the vorticity pattern with approximately the same magnitude.

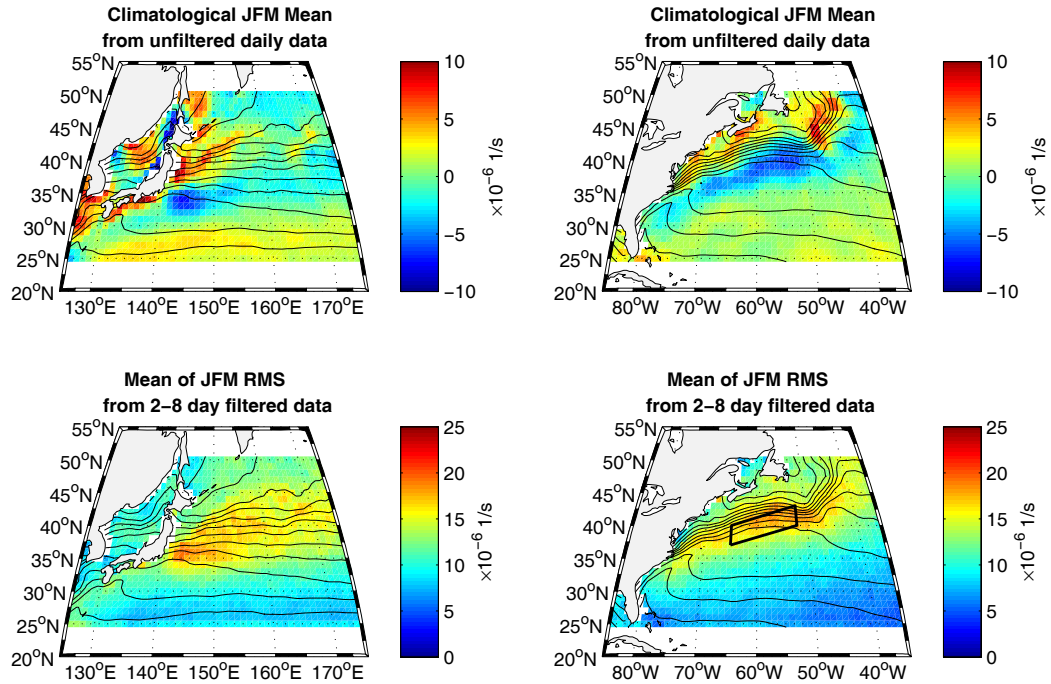


Figure 4. For the spatial regions shown in Figs. 2 and 3 (24.5:50.5N, -85.5:-34.5, or 124.5:175.5E), the winter root mean square (rms) synoptic variability in surface wind speed is plotted for the 22 year OAFlux record period. The solid lines are for the KE, the dashed for the GS. Smoothed interannual variability (with a symmetric, low-passed butterworth filter) is plotted with thicker lines to reduce interannual variability and better show the trends in the N. Pacific data. Linear trends using the unfiltered data are also shown.

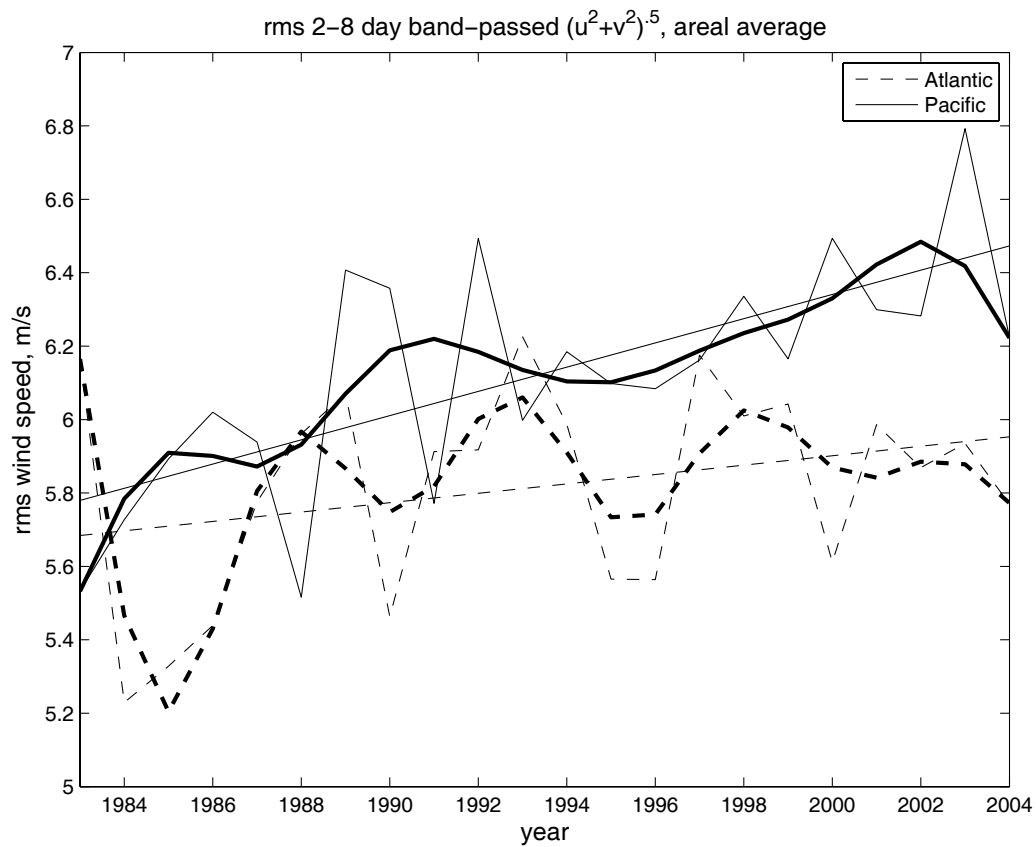


Figure 5. Normalized time series of the principal component of the GS latitude shift based upon subsurface temperature $T(200m)$ (dashed line), and satellite altimeter (solid line). Each of these PCs represent the leading EOF mode of seasonal ($T200m$) or monthly (altimeter) variability for the GS path. Only the JFM record for $T(200m)$ PC was used in our analysis.

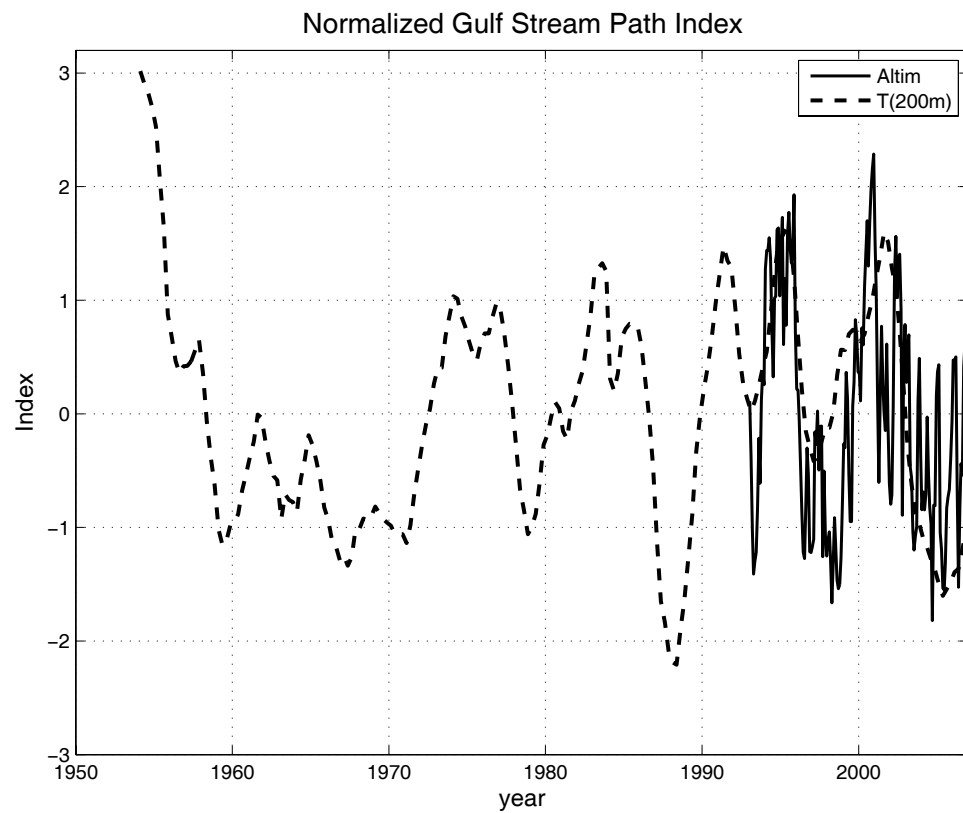


Figure 6. Normalized time series of KE path changes based upon SST (solid line), T(200m) (dashed line), and T(0:400m) (dotted line) subsurface temperatures as discussed in text.

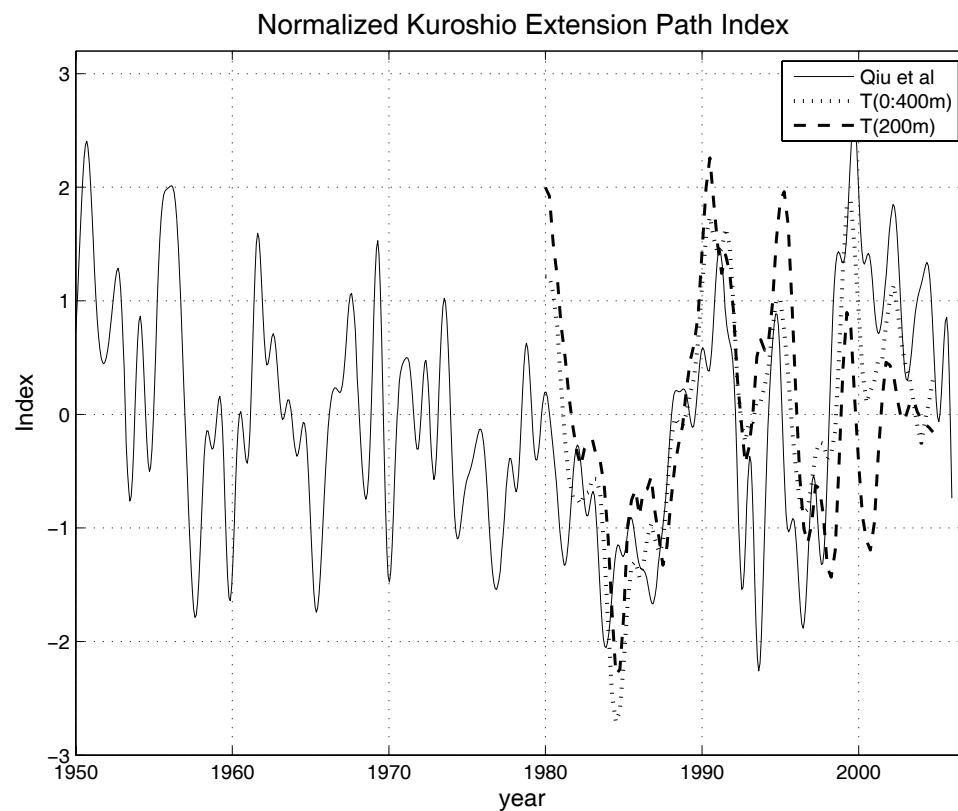


Figure 7. Latent heat flux for the GS region: mean rms 2:8 day band for JFM (upper left), interannual JFM std of rms 2:8 day band (lower left), correlation coefficient of interannual JFM rms variability with GS index (upper right) with only significant (>90%) values plotted, and regression against GS index (lower right). Darker shades of gray denote regions of positive correlation/regression here and elsewhere, while lighter shades of gray are negative. For all but the correlation coefficient, the units are in Wm^{-2} . The mean GS path is plotted as the solid line in all panels. The contour interval for the correlation coefficient (upper right) is 0.1 and for the regression is 0.1 times the gray scale maximum on the plot (lower right).

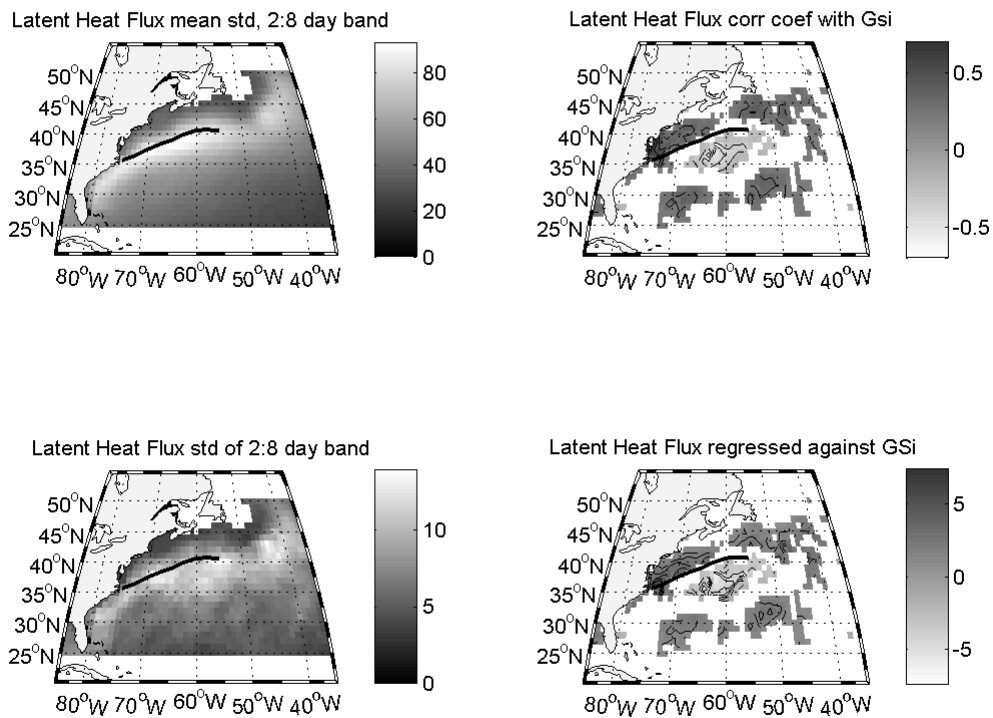


Figure 8. As in Fig. 7 but for Sensible Heat Flux.

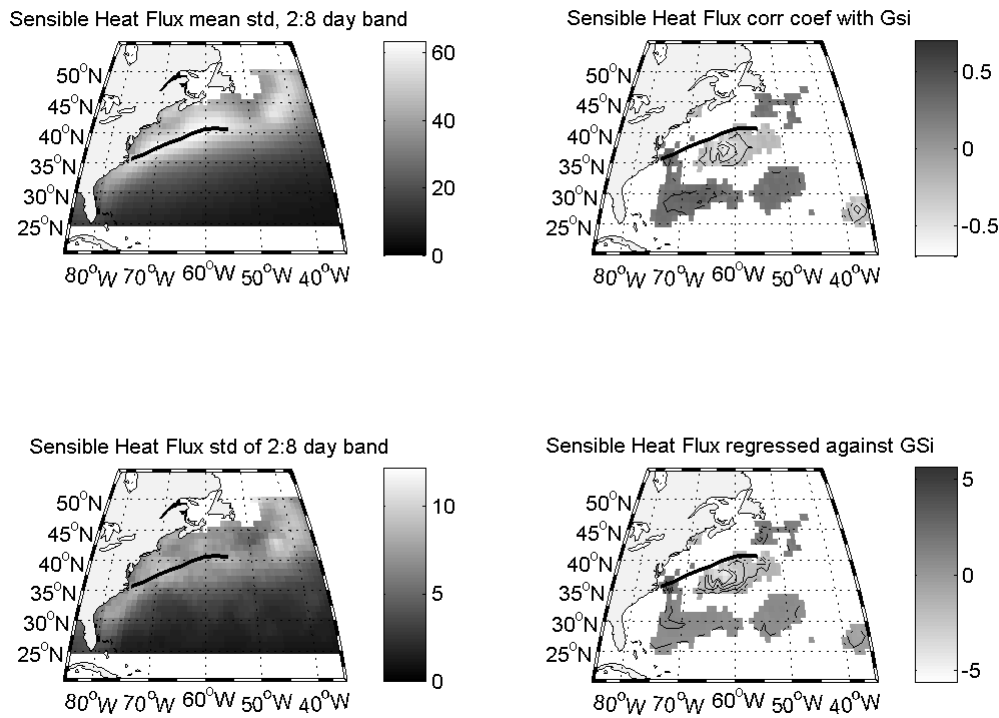


Figure 9. As in Fig. 7 but for Meridional Wind. In this case the units are in ms^{-1} .

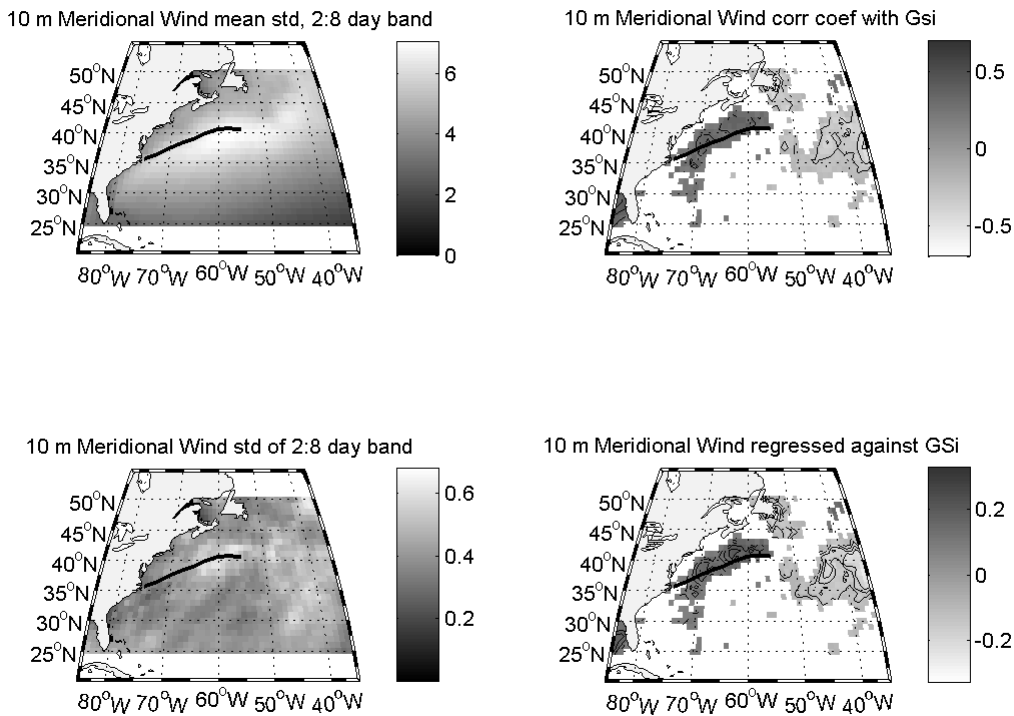


Figure 10. As in Fig. 7 but for Vorticity. For upper left panel, the scale is in 10^{-5} s^{-1} , while the scales for the lower left and lower right are in 10^{-6} s^{-1} .

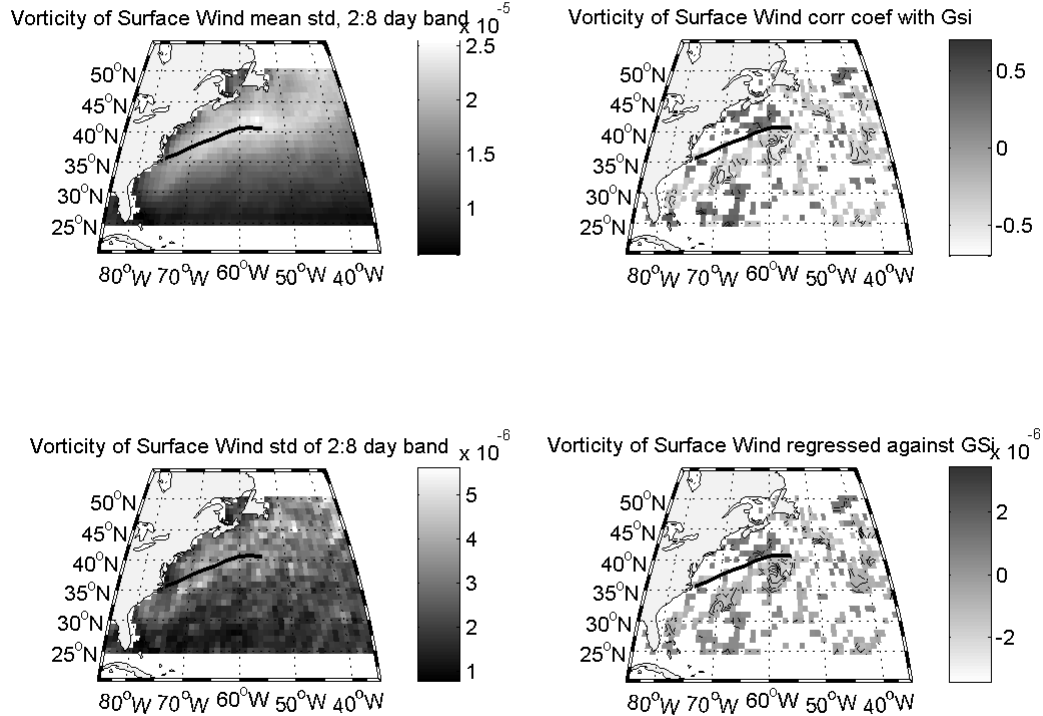


Figure 11. As for Fig. 10 but for Divergence.

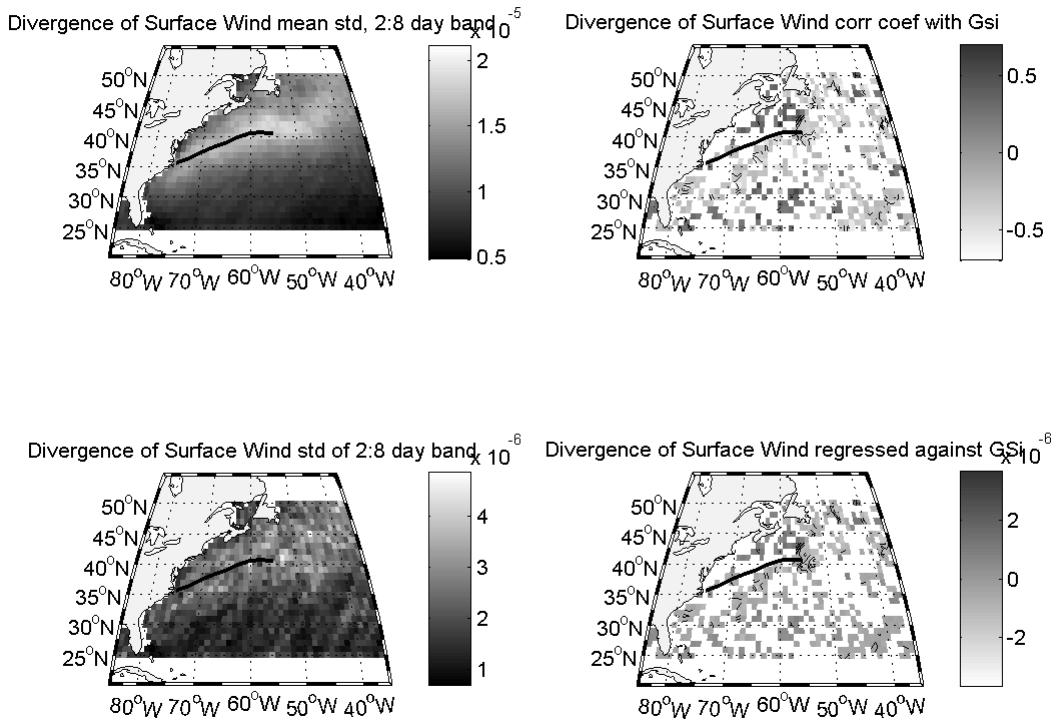


Figure 12. Latent Heat Flux for the KE region: mean rms 2:8 day band for JFM (upper left), interannual JFM std of rms 2:8 day band (lower left), correlation coefficient of interannual JFM rms variability with KE index (upper right) with only significant (>90%) values plotted, and regression against KE index (lower right). For all but the correlation coefficient, the units are in Wm^{-2} . The mean KE path is plotted as the solid line in all panels.

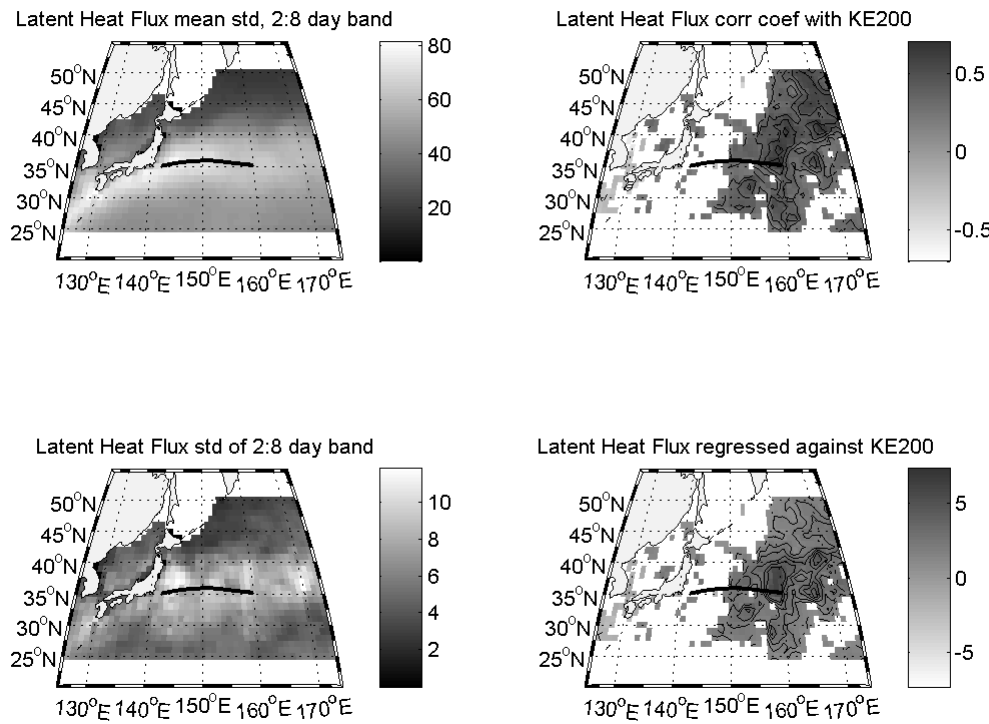


Figure 13. As in Fig. 12 but for Sensible Heat Flux.

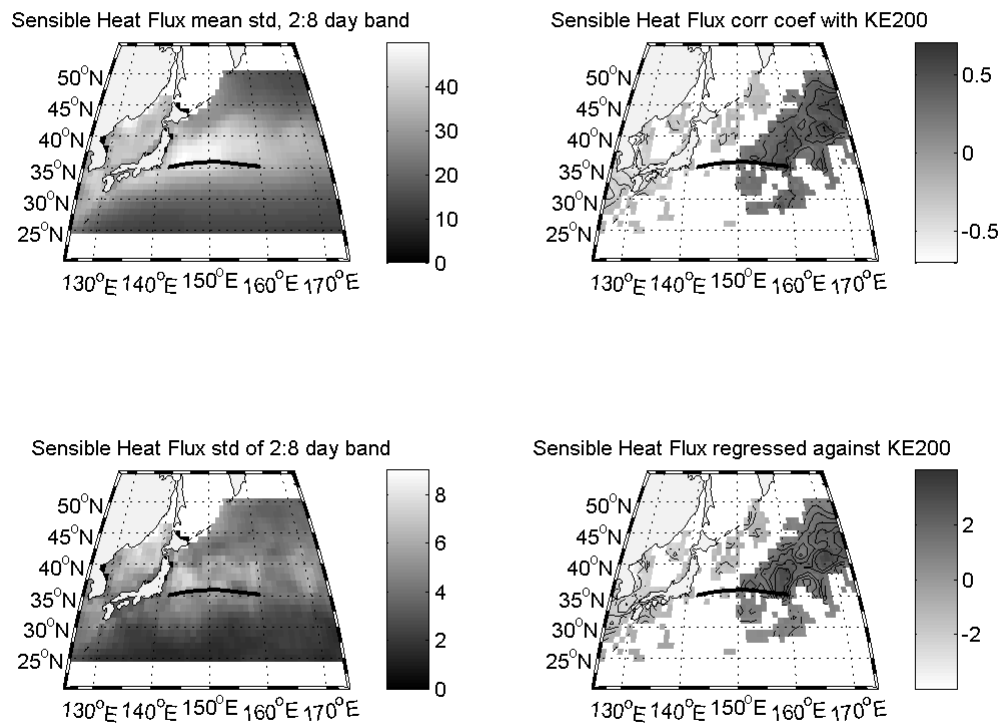


Figure 14. As in Fig. 12 but for Meridional Winds. In this case the units are in ms^{-1} .

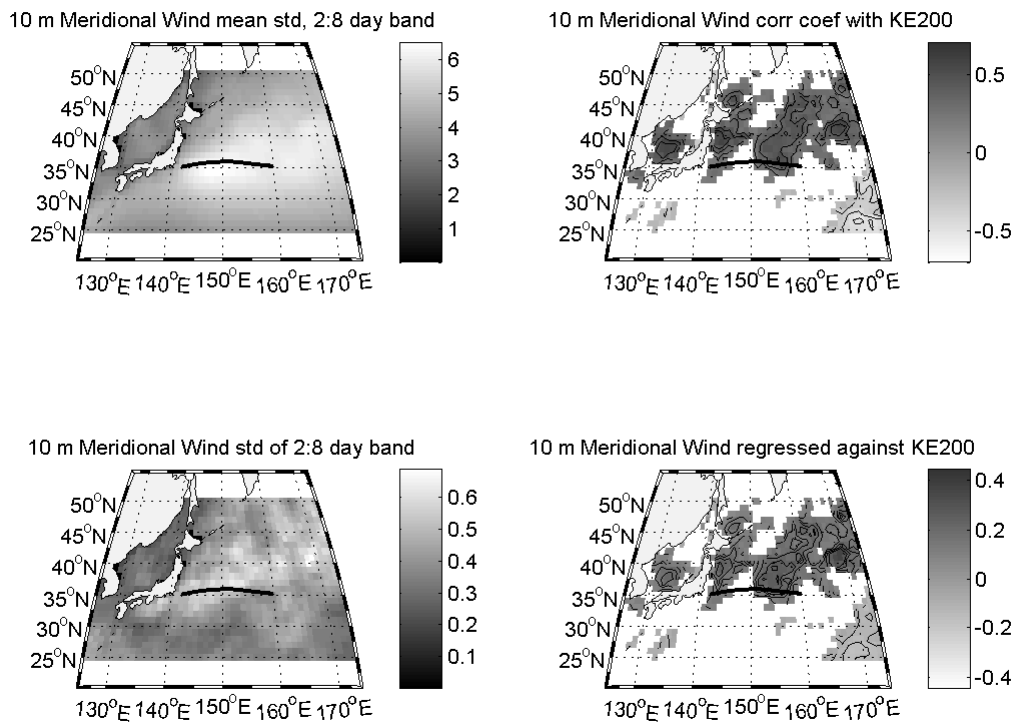


Figure 15. As in Fig. 10 but for vorticity in the KE region.

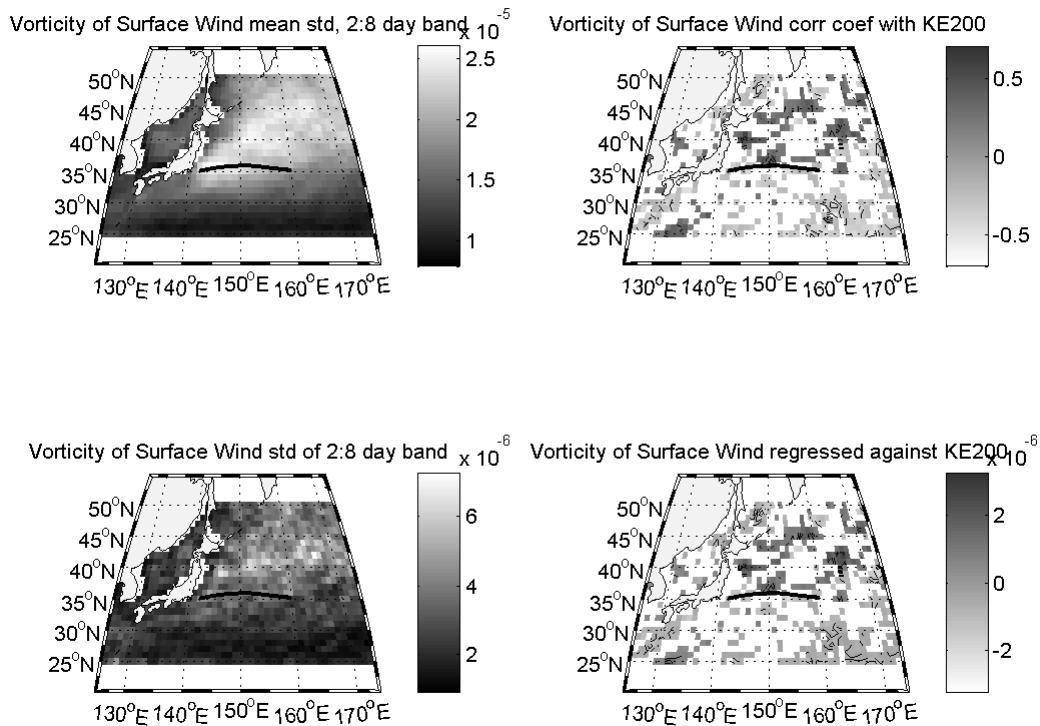


Figure 16. For the storm track maximum box over the GS (see Figs. 2, 3), we show a scatter plot of 2-8 day band-passed divergence and vorticity, with regression lines and % of variance explained by observations in each of the 4 quadrants of the plot (upper panel). The solid lines in the upper panel are regressions for one variable against the other. Along the neutral regression line (dashed in upper panel), we show the histogram of vorticity (lower panel) indicating a skewed distribution. Here we have filtered the data and removed the means, so the mean vorticity and divergence is zero. The means of these quantities are displayed in Figs. 2, 3, respectively.

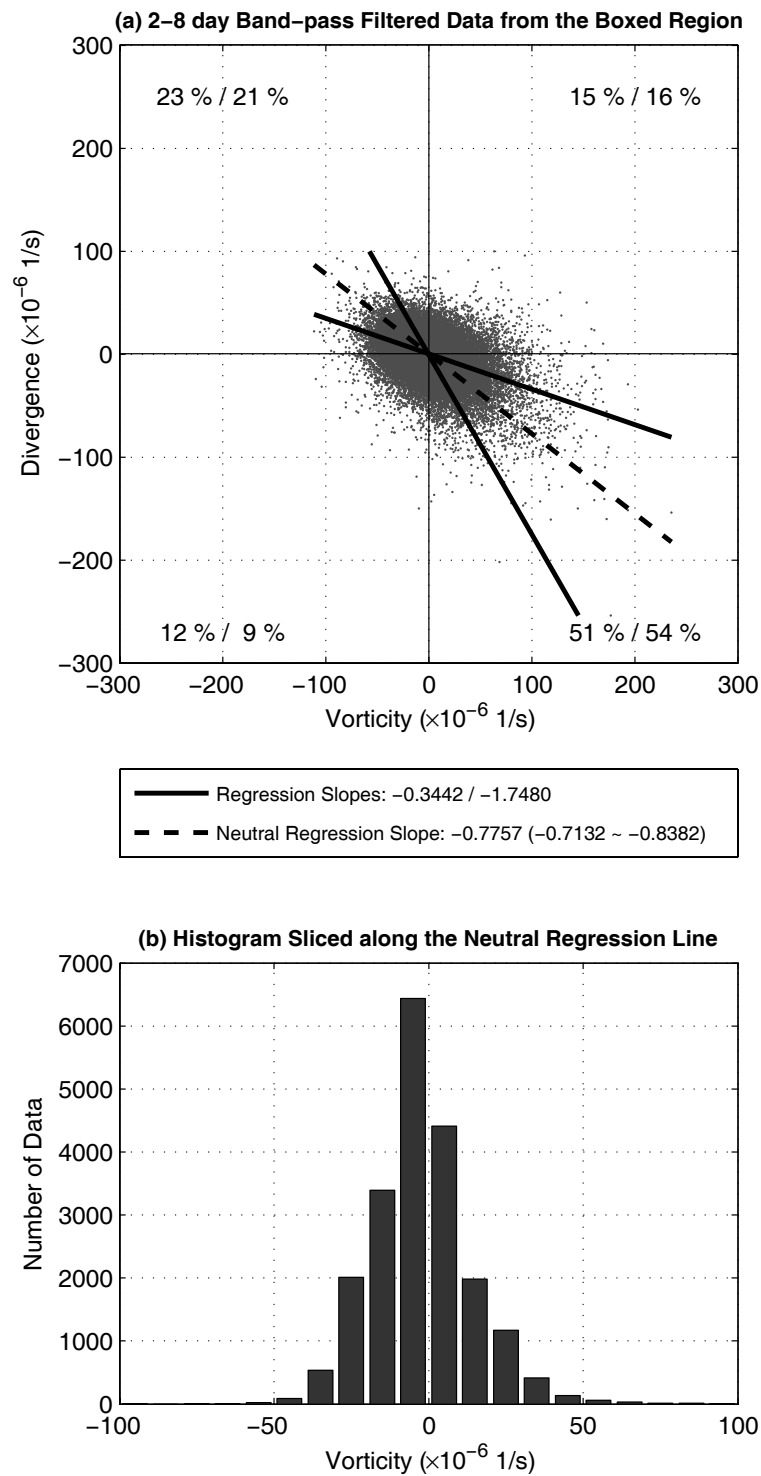


Figure 17. Wintertime SST signals are correlated with the KE and GS indices to show the effect of these frontal shifts on SST. The correlation coefficient (upper panels) is plotted for significant (>90% confidence) correlations and the regression ($^{\circ}\text{C}$, lower panels) is shown for the KE region (left panels) and GS (right panels). The contour interval for all panels is 0.1 in the respective units.

